Available online at www.sciencedirect.com

SciVerse ScienceDirect

Ceramics International 39 (2013) 7619–7625

CERAMICS INTERNATIONAL

www.elsevier.com/locate/ceramint

Synergistic effect of silane modified nanocomposites for active corrosion protection

K. Jeeva Jothi, K. Palanivelu*

Central Institute of Plastics Engineering and Technology (CIPET), Guindy, Chennai 600032, Tamil Nadu, India

Received 10 January 2013; received in revised form 4 March 2013; accepted 4 March 2013
Available online 13 March 2013

Abstract

This work presents an effective anticorrosion behavior of a hydrophobic surface on stainless steel 304. The protective coating has been designed by dispersing nanocomposites (cloisite 15A, multiwalled carbon nanotubes and cerium chloride) which act as a corrosion inhibitor. The sol was prepared by using 3-glycidoxypropyltrimethoxysilane (GPTMS), octyltriethoxysilane (OTES) and zirconium (IV) butoxide as precursors. The corrosion resistance of coated stainless steel got improved when nanocomposites were homogeneously embedded in silica sol. The influence of nano-particles on the barrier coatings impedes corrosion. The coatings were analyzed by X-ray diffraction (XRD) to ensure the intercalation and distribution of nanocomposites in layered silicates. Fourier transform infrared spectroscopy (FTIR) was employed to characterize the nanocomposites modified silica sol. Scanning electron microscopy (SEM) was used to examine the morphology of the modified silane coating. The contact angle measurements ensured the hydrophobic behavior of the coatings. The corrosion behavior was investigated using Electrochemical Impedance Spectroscopy (EIS). This study has led to a better understanding of active anticorrosive coatings with embedded nanocomposites and the factors influencing the anticorrosion performance.

Keywords: A. Films; A. Sol–gel processes; B. Nanocomposites; C. Corrosion; D. Clays

1. Introduction

The environment consists of different materials in contact with atmosphere. Many structural alloys corrode merely on exposure to moisture in air. Corrosion is the deterioration of a metal and is caused by the reaction of the metal with the environment especially moisture and impurities present in air. Stainless steel (SS) 304 is an important construction material widely used in the nuclear power plants (NPPs). However, it is susceptible to undesirable degradation in oxidizing environments. The oxide film formed on stainless steel plays a vital role in enhancing degradation resistance and buildup of radiation fields. Till now, some oxidation mechanisms have been proposed to elucidate the oxidation process [1]. There are many methods for rendering corrosion protection through surface engineering and one such is the use of sol–gel coatings.

Sol–gel technique is a simple process that employs low temperature curable coatings which are used for decorative purposes and also for surface protection. The surface protection mechanism could be based on providing a simple barrier coating (Inorganic and organic–inorganic hybrid-based), Inhibitor coating, sacrificial coating or a coating with self-healing property. The sol–gel technique introduces multi-functionality in the protective coatings and has been identified as a viable process for inhibitor coatings [2]. The most effective metal corrosion control technique consists of the electrical isolation of anode from the cathode [3,4]. The use of chromium oxide (Cr_2O_3) passivation layer formed on the surface of stainless steel in oxidizing environments has been reported and it guarantees a better durability and corrosion resistance of this particular alloy [5,6]. However, chromates are now heavily restricted in corrosion control procedures due to Cr (IV) toxicity and its carcinogenic nature. Due to this negative aspect a number of promising candidates, so called green inhibitors have been explored with the hope of replacing chromates. Among them, silane group of silicon based

*Corresponding author. Tel.: +91 44 2225 4701x06; fax: +91 44 2225 4707.
E-mail address: kpalanivelucipet@gmail.com (K. Palanivelu).

0272-8842/$ - see front matter © 2013 Elsevier Ltd and Techna Group S.r.l. All rights reserved.
http://dx.doi.org/10.1016/j.ceramint.2013.03.017

organic–inorganic chemicals has emerged as a very promising alternative [7]. The coating efficiency can be achieved by incorporation of some inhibitor like Ce^{3+} instead of the hazardous chromates. The Ce^{3+} inhibitor efficiency is a consequence of the redox couple Ce^{3+}/Ce^{4+}. The Ce^{4+} ions are converted into insoluble Ce (IV) hydroxide that precipitate at the cathodic sites of a corroding alloy and thus blocking the corrosion process [8]. Many researches are thus dealing with the combination of silanes with inhibitors (cerium) [9] or inhibitor nanocontainers [10]. Cerium nitrate added into the electrolyte showed an effective corrosion inhibiting effect on sol–gel based silane coating for magnesium alloy [11]. Hybrid sol–gel coatings loaded with corrosion inhibitor – cerium molybdate and 2-Mercaptobenzothiazole (MBT) has been reported [12]. Cerium is chosen as an inhibitor in most of the protective anti-corrosion coatings [13–19].

Carbon material, especially the Multiwalled Carbon Nanotubes (MWCNTs) are used as ideal reinforces for coatings due to their high strength, light weight, good geometrical properties, and also for their outstanding mechanical properties. Fabrication of well dispersed poly (N-vinylcarbazole) (PVK)/MWCNTs done via solution mixing process in different solvents have reported good anti-bacterial and anti-corrosive coating on metallic substrates [20,21]. Surface of nanotubes were modified by nitric acid [22] and by Dielectric Barrier discharge Plasma (DBP) [23]. MWCNTs have been used in coating for anti-bacterial application but more rarely in silica sol modification for corrosion barrier coatings.

A protective multilayer film formed by alternate layers of corrosion inhibitors poly cation bearing catechol group and nanoclay induces good barrier properties [24]. Meera et.al has reported that organically modified montmorillonite (MMT) sol–gel silica/nanoclay composites act as hydrophobic coating [25]. Nanocomposites membrane prepared using sulphonated poly (ether ether ketone) (SPEEK)/cloisite 15A shows good barrier properties [26]. In the comparative study of cloisite 15a and Cloisite Na^{+} for hydrophobic coatings using sol–gel method, cloisite 5A showed good result [27].

The aim of this paper is to incorporate the nanoclay, MWCNTs and cerium chloride into the hybrid silica sol for the development of protective sol–gel films protects stainless steel 304 with the help of inhibitors. These acts as nano-reservoirs and inhibitors embedded in the hybrid silica network which releases the active species under an external trigger. The results show that, coatings based on silane hybrid solutions improve the corrosion resistance of the stainless steel 304 substrate by the addition of nanomaterials as inhibitors. Further, the method proposed in this work is simple to apply and compatible with actual environmental.

2. Experimental

2.1. Materials

The chemicals and reagents used for the preparation of silica sols using the precursors, such as 3-glycidoxypropyltrimethoxysilane (GPTMS), octyltriethoxysilane (OTES) and zirconium (IV) butoxide from Aldrich®, 2-butoxy ethanol ($C_6H_{14}O_2$) and hydrochloric acid (HCl) from MERCK. Cerium (III) chloride ($CeCl_3$) from Avra Synthesis, nanoclay (Cloisite 15A) from Southern Clay Products, Multiwalled Carbon Nanotubes (MWCNTs) from Sharda Enterprises and double distilled water were used throughout the experiments.

2.2. Preparation of sol

The sol was prepared by adding the chemicals such as GPTMS, OTES, 2-butoxy ethanol and zirconium (IV) butoxide in the ratio of 3:1:11:1respectively in 0.1 M HCl. The solution was stirred at room temperature for 24 h. The resultant sol was clear and homogeneous solution and is referred to be as GZ. To the three parts of above solution, 1% by weight each of cloisite 15A, MWCNTs and $CeCl_3$ were added and these sols are referred to as GZ-15A, GZ-CNT, and GZ-Ce, respectively. A pretreatment was carried out for cloisite 15A and MWCNTs and not for cerium chloride.

2.2.1. Pretreatment of MWCNTs

MWCNTs were functionalized by nitric acid [28]. MWCNTs were preheated to 100 °C for 2 h. Then 4 M HNO_3 was added to the preheated MWCNTs in the ratio 3:1 by weight. The mixture was then boiled at 100 °C for 2 h and washed with distilled water to give neutral pH. The sample was then dried in oven for 2 h and sonicated in the ratio 1:36 of MWCNTs with acetone. It was dried and manually grinded in a mortar.

2.2.2. Pretreatment of cloisite 15A

Before the addition of cloisite 15A to the silica sol it was dried in an oven at 60 °C overnight and ultrasonicated with acetone for 20 min. Again it is dried in the oven and manually grinded in a mortar. With the help of an ultrasonicator the MWCNTs and cloisite 15A were dispersed to avoid agglomeration in the coatings.

2.3. Substrate and coating deposition

The substrate used for the present investigation is stainless steel 304. The chemical composition of stainless steel 304 alloy is given in the Table 1.

The substrates with dimensions of 20 mm×40 mm×1 mm were polished with emery papers of finer grit down to 1200. The polished substrates were washed with distilled water and acetone to remove all the dirt and grease. It was then dried in air. The cleaned substrates were dipped into the sol for duration of 10–15 s at a withdrawal speed of 170 mm/min. The films were dried at room temperature for 20 min, to

Table 1
Chemical composition of stainless steel 304 (wt%).

C	Mn	P	S	Si	Cr	Ni	Al	Fe
0.08	2.00	0.045	0.030	0.750	20.0	10.5	0.1	Balance

parturitate the chemical bonds between the deposited sol and the substrate. The films were then annealed at 120 °C for 1 h. The silica films thus formed were taken out of the oven and cooled at room temperature.

2.4. Characterization technique

The films were characterized by Fourier transform infrared spectroscopy (FTIR) (Avatar 303) which gave the information about various chemical bonds such as O–H, Si–C, C–H, and Si–O–Si. Thermogravimetric Analysis (TGA) (Perkin Elmer) was carried out to know the thermal stability of the films by heating the samples from 30 °C to 900 °C at a heating rate of 10 °C/min with N_2 flow of 20 mL/min. The surface morphology of the silica/modified nanocomposites coatings were studied with the help of Scanning Electron Microscopy (SEM, ZEISS, EVO MA15). The crystallographic patterns of coated films were analyzed by using X-ray diffractometer (Shimadzu, XD-D1 diffractometer). The basal spacing was derived from the peak position in the XRD diffractogram. Polarization tests were carried out for SS 304 substrates in 0.5 M NaCl solution. Prior to the measurements, the samples were kept in the working solution for a minimum of half an hour in order to reach a steady potential. The potentiodynamic measurements were taken within the range of potential −0.5 to +2.5 mV. Salt spray technique was carried out using 3.5% NaCl solution at 35 °C, in a Salt Spray Chamber supplied by ATLAS.

3. Results and discussion

FT-IR spectra of GZ, GZ-15A, GZ-CNT and GZ-Ce are shown in Fig. 1. In the figure it is clear that after modifying the surface with nanocomposites adsorption band corresponding to O–H (around 3425 cm^{-1}) decreases slowly. The characteristic bands at 1030, 779 and 464 cm^{-1} corresponds to the stretching, bending and out of plane bending of Si–O bonds, respectively. Peaks in the spectral range around 1629 cm^{-1} can be attributed to C–O bending. The adsorption peaks at 2927 cm^{-1} and 2863 cm^{-1} are associated with C–H stretching modes which indicate the presence of long alkyl groups in the silica network. The bands at 2926 cm^{-1} and 2861 cm^{-1} show the C–H asymmetric and symmetric stretching frequencies, and that at 1462 cm^{-1} and 694 cm^{-1} corresponds to C–H symmetric and asymmetric bending, respectively. In the Fig. 1c, a new medium transmittance band at 2371 cm^{-1} indicates the presence of CO and CO_2 groups. CO and CO_2 groups apparently exhibit the peaks in the range 2100–2400 cm^{-1} [29]. The peak at 1627 cm^{-1} can be associated with the stretching of MWCNTs backbone [30]. The O–H band in GZ-Ce got decreased compared to GZ, GZ-15A and

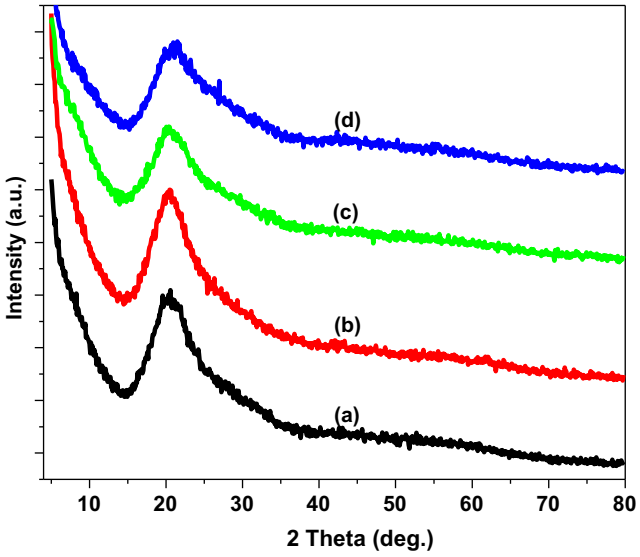

Fig. 2. XRD patterns for: (a) GZ, (b) GZ-15A, (c) GZ-CNT, and (d) GZ-Ce.

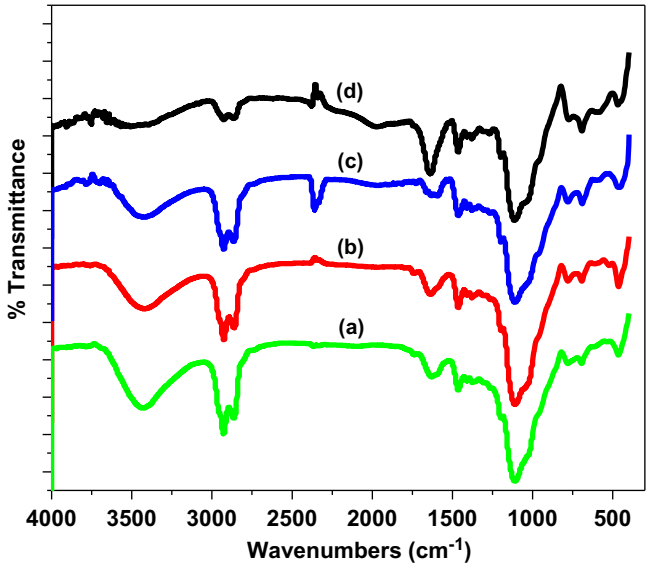

Fig. 1. FT-IR spectra for: (a) GZ, (b) GZ-15A, (c) GZ-CNT, and (d) GZ-Ce.

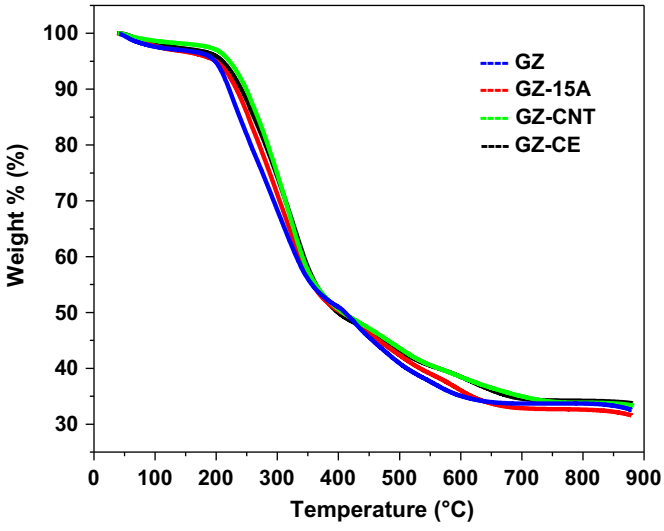

Fig. 3. TGA curves for GZ, GZ-15A, GZ-CNT and GZ-Ce.

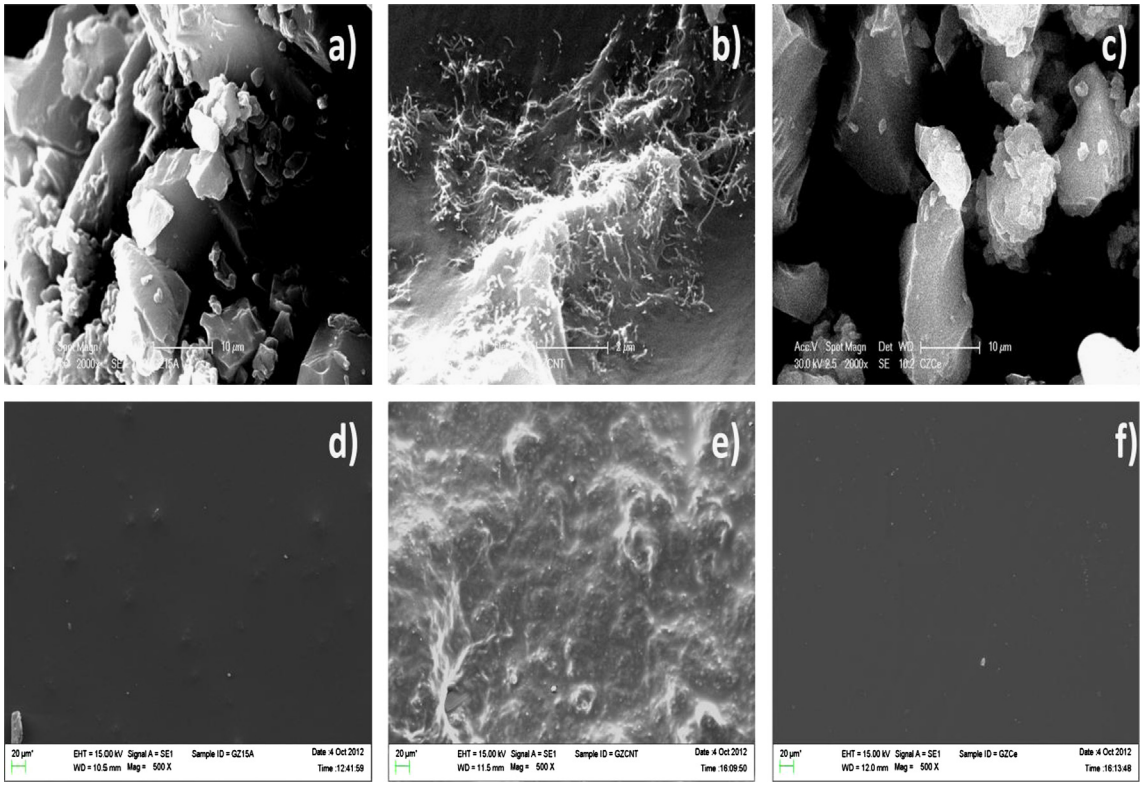

Fig. 4. Surface morphology studies for (a) GZ-15A, (b) GZ-CNT, (c) GZ-Ce in powder form and (d) GZ-15A, (e) GZ-CNT, (f) GZ-Ce shows that materials coated on SS surface.

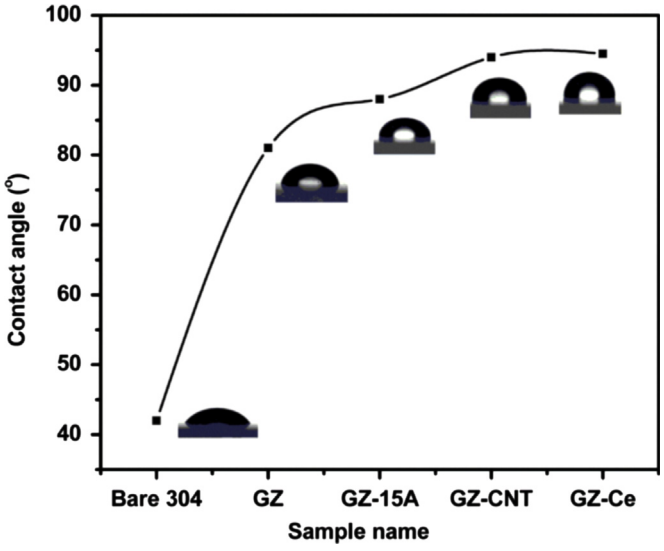

Fig. 5. Contact angle images for uncoated and coated stainless steel substrates.

GZ-CNT, which confirms that silica surface with Si–OH groups were replaced by hydrolytically stable group through oxygen bonds that prevents the adsorption of water and hence results in the hydrophobic silica surface. Peaks at 2926 and 2865 cm^{-1} corresponds to C–H stretching mode also got decreased compared to other peaks. The strong band observed at 1112 cm^{-1} indicates the presence of Si–O–Si moiety. The peak at 465 cm^{-1} corresponds to the symmetric bending of SiO_2. Bands at 778 and 1276 cm^{-1} are due to the Si–CH_3 groups. The appearance of band 1276 cm^{-1} in Fig. 1d corresponds to increased amount of Si–CH_3 which is different from other spectra.

XRD patterns show only one broad peak at around 20 deg that corresponds to the typical diffraction of amorphous SiO_2 group (d_{001}). According to the literature XRD patterns for MWCNTs revealed the presence of peak at 25.6 deg corresponds to d_{002} for nanotubes and d_{100} for carbon atoms respectively [31]. In the case of cloisite 15A, $2\theta = 2.6$ deg and 7.1 deg corresponds to the incorporation of tallow molecules that have been commercially introduced into the clay structure and reflection at the plane d_{001} respectively [26]. The concentration of nanocomposites were quite low, so no clear peaks was observed after the addition of cloisite 15A, MWCNTs and cerium chloride as shown in the Fig. 2.

Thermal stability of prepared sol–gel silica/nanocomposites was determined using TGA as shown in the Fig. 3. TGA studies have been used to relate the dispersion behavior of nanocomposites in a silica matrix. It can be seen from the thermogram that initial weight loss from 30 °C to 150 °C corresponds to the evapouration of residual free water and ethanol from the silica gel nanocomposites. The weight loss above 150 °C is due to loss of water present in the micro pores and some hydroxyl groups from the sol–gel network. The thermogram of organic and inorganically modified nanocomposites shows a weight loss above 200 °C may be due to the evapouration of hydroxyl residue. The thermogram of sol–gel silica/modified nanocomposites shows increase in degradation temperature after the addition of cloisite 15A, MWCNT and

Fig. 6. Corrosion tested substrate after 432 h in the salt spray chamber (a) Bare SS 304, (b) GZ, (c) GZ-15A, (d) GZ-CNT, and (e) GZ-Ce coated samples.

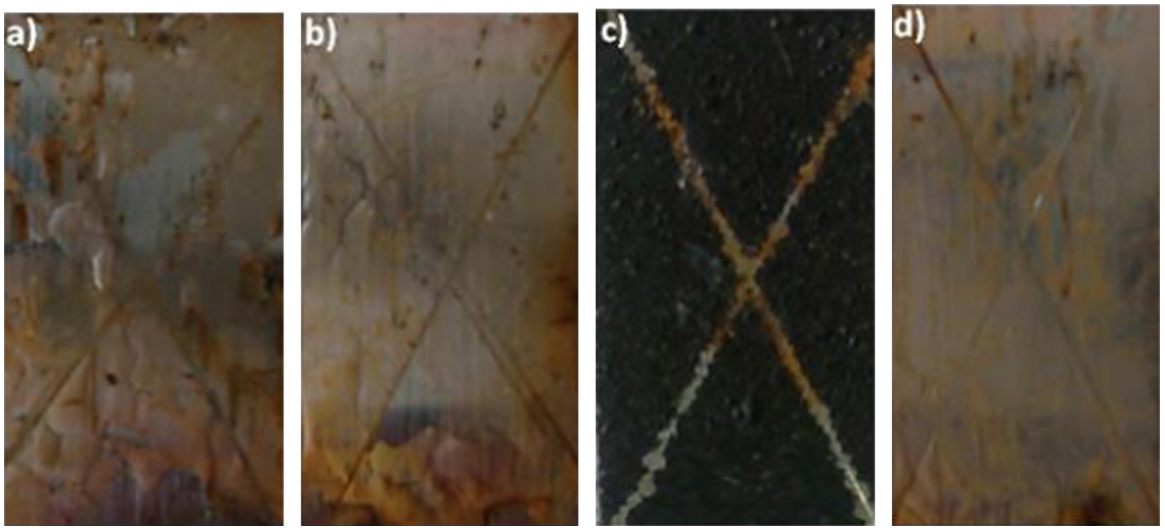

Fig. 7. Durability tested samples after 40 days of immersion in tape water (a) GZ, (b) GZ-15A, (c) GZ-CNT and (d) GZ-Ce.

$CeCl_3$. This reveals that the dispersion of nanocomposites in silica network has increased its thermal stability. The improvement in the degradation temperature may be due to the homogeneous dispersion of nanocomposites, which ionically interacted with the silica network and hinders the decomposition of the materials.

Surface morphologies of the prepared sol–gel composites were examined using SEM analysis as shown in the Fig. 4. The surface morphology of the powdered silica gel with cloisite 15A in the Fig. 4a shows the layered surface with large flakes due to the presence of montmorillonite; whereas Fig. 4d shows the coated surface of GZ-15A appearing as smooth, evenly distributed nanoclay with micro size silica lumps at few places. MWCNTs are well dispersed in the silica matrix as shown in the Figs. 4b and e shows the silica coated surface modified by MWCNTs, which appear to be slightly rough. The MWCNTs gets rooted in the silica matrix and covers the surface by protecting it from corrosion. Fig. 4c shows the typical SEM image of powdered cerium doped silica with layered flakes and its coating in Fig. 4f seems to be uniform, smooth, defect and crack-free when compared to other two composite coatings.

Fig. 5 shows the hydrophobicity of the film surfaces after the addition of nanocomposites. The octyl group present in OTES contributes to the hydrophobicity of the film. The contact angle of SS 304 abruptly increases from 42 deg to 81 deg on coating. However, using OTES as co-precursor the –OH groups get replaced by hydrolytically stable –O–Si-octyl group and these groups are modified by the nanocomposites to make the surface hydrolytically stable and protect it from corroding. The contact angle of GZ-15A, GZ-CNT and GZ-Ce were 89 deg, 94 deg and 95 deg, respectively. This

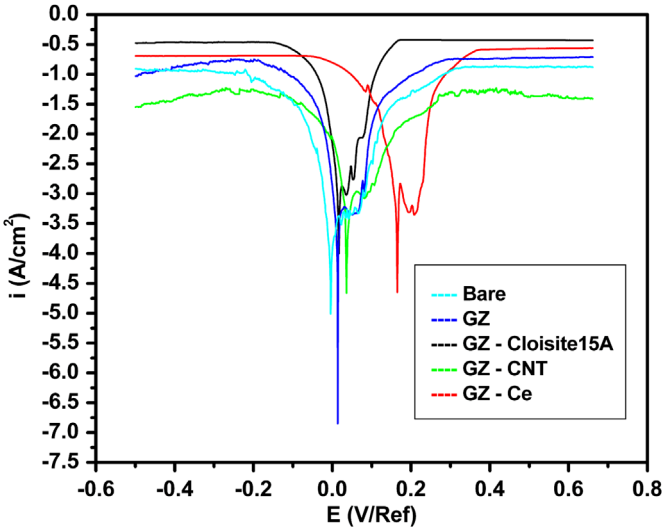

Fig. 8. Tafel plots for uncoated and coated stainless steel substrates in aerated 0.5 M NaCl.

shows that the surface becomes more hydrophobic after the addition of nanocomposites which minimizes the surface free energy. This imparts antiwetting property to the resultant hybrid films and prevents it from corroding. Cerium doped silica coating shows little higher contact angle compared to the other coatings because of the low surface tension.

The traditional salt spray technique was used to investigate the corrosion performance of the sol–gel films coated on stainless steel 304. The coated plates were exposed in salt spray chamber for 432 h (18 days) are shown in the Fig. 6 (taped areas were cropped and specifically corrosion affected portion were taken). It can be clearly seen that silane doped cerium surfaces exhibit less corrosion and retain their original shiny surface. The bare SS 304 on contrast exhibits early signs of corrosion. Therefore, the data confirms that cerium doped silane coatings have good anti-corrosion property. Cerium doped silane coating shows the highest hydrophobic behavior facilitating the corrosion inhibition compared to cloisite 15A and MWCNTs modified silane coatings.

For durability test, the uncoated and coated samples were immersed in ordinary tap water (pH = 8.5) for longtime and in order to find out how many days the coatings can with stand. After 40 days of immersion the GZ, GZ-15A and GZ-CNT surfaces got peeled off while GZ-Ce coating remain intact as shown in the Fig. 7.

The Electrochemical Tafel Slope Analysis was performed to evaluate the anticorrosion performance of GZ, GZ-15A, GZ-CNT, GZ-Ce as well as uncoated stainless steel 304 substrates. The Tafel plots for uncoated and coated samples were recorded by sweeping of the potential from equilibrium potential toward negative and positive potential against Ag/AgCl reference electrode in NaCl (0.5M) electrolyte. Fig. 8 shows the Tafel plots for uncoated and coated substrates and Table 2 gives the corrosion potential (E_{corr}) and corrosion current (I_{corr}) values as obtained from the Tafel slopes. When compared to the bare SS 304, the substrate which is coated has a positive shift in the E_{corr} value. In addition, the I_{corr} value also got decreased from 5.65 to 2.1×10^{-2} μA cm^{-2}. These results show that the GZ coating can block the moisture and oxygen and thus corrosion can be suppressed effectively. Furthermore, to improve the performance of corrosion protection to a larger extent I_{corr} values can be lowered by adding cloisite 15A, MWCNTs and cerium chloride to the silica network as represented in Table 2. So, the sol–gel hybrid coating significantly reduces the value of estimated corrosion current compared to that of uncoated substrates. The results reveal that the surface coated with GZ-Ce exhibits better performance in corrosion protection.

Table 2
Electrochemical parameters (corrosion potential and corrosion current) obtained from the polarization measurements in 0.5 M of NaCl solution.

Sample	E_{corr} (mV)	I_{corr} (μA/cm^2)
Uncoated	−0.006	5.65
GZ	0.011	2.1×10^{-2}
GZ-15A	0.016	2.8×10^{-3}
GZ-CNT	0.033	1.2×10^{-3}
GZ-Ce	0.166	4.2×10^{-4}

4. Conclusion

To conclude the anti-corrosive property of stainless steel 304 coated with silane modified with cloisite 15A, MWCNTs and $CeCl_3$, were studied for barrier enhancing properties. The results of FTIR analysis indicated the formation of a denser siloxane network with nanocomposites. In addition, SEM analysis confirmed the formation of homogenous film on the surface of substrate without any defect due to intercalation of nanocomposites. The water repellent property of the hydrophobic surface acts as a barrier for water or other aggressive species from reaching the metal and thus preventing the oxidation of the metal surface. Silica sol doped with cerium showed higher contact angle which imparts better anti-wetting property for the hybrid films when compared to other modifications. The result of electrochemical analysis and the salt spray test showed that GZ-Ce has good barrier properties for silane films and increased anodic polarization compared to other coated and uncoated substrates. These results when combined with the whole green building process will make our strategy attractive and promising for replacing the banned highly toxic chromic treatments with silica. However progress has to be made to have the same level of protection for metal surfaces than these treatments and to understand the synergistic effect of silane hybrid nanocomposites on the metal surface for protection.

Acknowledgments

The authors are grateful to Defence Research and Development Organization (DRDO), Government of India, New Delhi for their financial support.

References

[1] W. Kuang, X. Wu, E.H. Han, Influence of dissolved oxygen concentration on the oxide film formed on 304 stainless steel in high temperature water, Corrosion Science 63 (2012) 259–266.
[2] N. Kumar, R. Subasri, Corrosion protection and self-healing by sol–gel process: a review of recent patent literature, Recent Patents on Corrosion Science 2 (2) (2012) 148–163.
[3] D.A. Jones, Principles and Prevention of Corrosion, 2nd ed., Prentice-Hall, New Jersey, 1996.
[4] L.L. Shreir, R.A. Jarman, G.T. Burstein (Eds.), 3rd ed., Butterworth-Henemann, Oxford, 1994.
[5] R.A. Buchheit, Compilation of corrosion potentials reported for intermettalic phases in aluminum alloys, Journal of the Electrochemical Society 142 (1995) 3994–3996.
[6] T.P. Chou, C. Chandrasekaran, S. Limmer, C. Nguyen, G.Z. Cao, Organic–inorganic sol–gel coating for corrosion protection of stainless steel, Journal of Materials Science Letters 21 (2002) 251–255.
[7] W.J. Van Ooij, D. Zhu, V. Palanivel, J.A. Lamar, M. Stacy, The potential of silanes for chromate replacement in metal finishing industries, Silicon Chemistry 3 (2006) 11–30.
[8] K.A. Yasakau, M.L. Zheludkevick, S.V. Lamaka, M.G.S. Ferreira, Mechanism of corrosion inhibition of AA2024 by rare-earth compounds, Journal of Physical Chemistry B 110 (11) (2006) 5515–5528.

[9] L.S. Kasten, J.T. Grant, N. Grebash, N. Voevodin, F.E. Arnold, M.S. Donley, An XPS study of cerium dopants in sol–gel coatings for aluminum 2024-T3, Surface and Coatings Technology 140 (2001) 11–15.
[10] M.F. Montemor, W. Trabelsi, S.V. Lamaka, K.A. Yasakau, M.G.S. Ferreira, The synergistic combination of bis Silane and CeO_2–ZrO_2 nanoparticles on the electrochemical behavior of galvanized steel in NaCl solution, Electrochimica Acta 53 (20) (2008) 5913–5922.
[11] F. Luo, Q. Li, X.K. Zhong, H. Gao, Y. Dai, F.N. Chen, Corrosion electrochemical behaviours of silane coating coated magnesium alloy in NaCl solution containing cerium nitrate, Materials and Corrosion 63 (2) (2012) 148–154.
[12] I.A. Kartsonakis, A.C. Balaskas, E.P. Koumoulos, C.A. Charitidis, G.C. Kordas, Incorporation of ceramic nanocontainers into epoxy coatings for the corrosion protection of hot dip galvanized steel, Corrosion Science 57 (2012) 30–41.
[13] S. Kozhukharov, V. Kozhukharov, M. Schem, M. Aslan, M. Wittmar, A. Wittmar, M. Veith, Protective ability of hybrid nano-composite coatings with cerium sulphate as inhibitor against corrosion of AA2024 aluminium alloy, Progress in Organic Coatings 73 (2012) 95–103.
[14] D. Balgude, A. Sabnis, Sol–gel derived hybrid coatings as an environment friendly surface treatment for corrosion protection of metals and their alloys, Journal of Sol–Gel Science and Technology 64 (1) (2011) 124–134.
[15] E. Gonzalez, J. Pavez, I. Azocar, J.H. Zagal, X. Zhou, F. Melo, G.E. Thompson, M.A. Páez, A silanol-based nanocomposite coating for protection of AA-2024 aluminium alloy, Electrochimica Acta 56 (2011) 7586–7595.
[16] L. Paussa, F. Andreatta, N.C. Rosero Navarro, A. Durán, L. Fedrizzi, Study of the effect of cerium nitrate on AA2024-T3 by means of electrochemical micro-cell technique, Electrochimica Acta 70 (2012) 25–33.
[17] X. Zhong, Q. Li, J. Hu, X. Yang, F. Luo, Y. Dai, Effect of cerium concentration on microstructure, morphology and corrosion resistance of cerium silica hybrid coatings on magnesium alloy AZ91D, Progress in Organic Coatings 69 (2010) 52–56.
[18] R.V. Lakshmi, G. Yoganandan, K.T. Kavya, B.J. Basu, Effective corrosion inhibition performance of Ce^{3+} doped sol–gel nanocomposites coating on aluminum alloy, Progress in Organic Coatings, in press.
[19] S. Kozhukharov, V. Kozhukharov, M. Wittmar, M. Schem, M. Aslan, H. Caparrotti, M. Veith, Protective abilities of nanocomposites coatings containing Al_2O_3 nano-particles loaded by $CeCl_3$, Progress in Organic Coatings 71 (2011) 198–205.
[20] K.M. Cui, M.C. Tria, R. Pernites, C.A. Binag, R.C. Advincula, Carbon nanotube poly(N-vinyl carbazole) electropolymerized conjugated polymer network (CPN) nanocomposite films, ACS Applied Materials & Interfaces 3 (7) (2011) 2300–2308.
[21] C.M. Santos, K.M. Cui, F. Ahmed, M.C.R. Tria, R.A.M.V. Vergara, A.C.D. Leon, R.C. Advincula, D.F. Rodrigues, Bactericidal and anticorrosion properties in PVK/MWNT nanocomposite coatings on stainless steel, Macromolecular Materials and Engineering 297 (2012) 807–813.
[22] I.D. Rosca, F. Watari, M. Uo, T. Akasaka, Oxidation of multiwalled carbon nanotubes by nitric acid, Carbon 43 (2005) 3124–3131.
[23] M.V. Naseh, A.A. Khodadadi, Y. Mortazavi, O.A. Sahraei, F. Pourfayaz, S.M. Sedghi, Functionalization of carbon nanotubes using nitric acid oxidation and DBD plasma, WASET 49 (2009) 177–179.
[24] E. Faure, E. Halusiak, F. Farina, N. Giamblanco, C. Motte, M. Poelman, C. Archambean, C.V. Weerdt, J. Martial, C. Jerome, A.S. Duwez, C. Detrembleur, Clay and DOPA containing polyelectrolyte multilayer film for imparting anticorrosion properties to galvanized steel, Langmuir 28 (2012) 2971–2978.
[25] K.M.S. Meera, R.M. Sankar, A. Murali, S.N. Jaisankar, A.B. Mandal, Sol–gel network silica/modified montmorillonite clay hybrid nanocomposites for hydrophobic surface coatings, Colloids and Surfaces B 90 (2012) 204–210.
[26] J. Jaafar, A.F. Ismail, T. Matsuura, Preparation and barrier properties of SPEEK/Cloisite15A®/TAP nanocomposites membrane for DMFC application, Journal of Membrane Science 345 (2009) 119–127.
[27] K. Jeeva Jothi, K. Palanivelu, Effect of nanoclays on silica network for hydrophobic coatings by sol–gel method, Applied Clay Science, in press.
[28] F.A. Abuilaiwi, T. Laoui, M. Al-Harthi, M.A. Atieh, Modification and functionalization of multiwalled carbon nanotubes (MWCNT) via Fisher esterification, Arabian Journal for Science and Engineering 35 (2010) 37–48.
[29] N.B. Asari-Mansor, J.P. Tessonnier, A. Rinaldi, S. Reiche, M.G. Kutty, Chemically modified multiwalled carbon nanotubes (MWCNTs) with anchored acidic groups, Sains Malaysiana 41 (5) (2012) 603–609.
[30] S. Goyanes, G.R. Rubiolo, A. Salazar, A. Jimeno, M.A. Corcuera, I. Mondragon, Carboxylation treatment of multiwalled carbon nanotubes monitored by infrared and ultraviolet spectroscopies and scanning probe microscopy, Diamond and Related Materials 16 (2007) 412–417.
[31] C. Pirlot, I. Willems, A. Fonseca, J.B. Nagy, J. Delhalle, Preparation and characterization of carbon nanotube/polyacrylonitrile composites, Advanced Engineering Materials 4 (2002) 109–114.